第 43 卷 第 1 期/2023 年 1 月/光学学报 研究论文

光学学报

基于复合旋转光力系统的非线性光学特性研究

陈咏雷，陈华俊*，刘云鹤，谢宝豪

安徽理工大学力学与光电物理学院，安徽 淮南 232001

摘要 研究了由探测光和泵浦光同时驱动下的复合旋转光力系统中的非线性行为，如光学双稳态行为和四波混频(FWM)现象。通过操控光力腔旋转速率大小和方向能有效调控旋转诱导产生的 Sagnac 频移大小，进而能有效操控光学双稳态行为。进一步研究了该系统中的FWM现象，发现光力腔的旋转方向和旋转速率都会影响系统的FWM强度谱线，同时FWM强度减小或增大会加剧或抑制系统共振区域的模式分裂现象。此外，还探讨了外力对复合旋转光力系统中FWM现象的影响，发现：外力会破坏系统FWM强度谱的对称性，并且在同一旋转速率下，外力的增强会使得FWM强度显著增大；在同一外力下，旋转速率的增大会降低系统的FWM强度。

关键词 非线性光学；旋转光力系统；Sagnac效应；光学双稳态；四波混频

中图分类号 O436 **文献标志码** A **DOI**：10.3788/AOS221068

1 引 言

腔光力学系统[1-2]通过腔内辐射压力来描述空腔内光场与机械振子之间的相互作用，是过去十几年里量子光学中发展较为迅速的领域，在高精度测量[3-10]、纳米机械振子基态冷却[11-15]和量子信息处理[16-19]等方面有潜在的应用并取得了重大突破。近年来，许多有趣的光学非线性现象被发现，如光学双稳态[20-23]、光力诱导透明[24-27]、电磁感应透明[28]、二阶边带[29-30]、高阶边带[31-32]、快慢光效应[33-35]和四波混频(FWM)[36-40]等。光学双稳态是指对系统施加的功率可以提供两种不同的输出，其本质是辐射压力和机械振子之间耦合的非线性性质[41-42]。值得一提的是，实验上首次观察到了强激光场可以控制系统的光学双稳态[43]。随后，光学双稳态现象在许多光力系统中被观测到，如量子阱光力系统[44]、玻色-爱因斯坦光力系统[45-46]和复合光力系统[47-48]。FWM现象可以描述为当用一束泵浦光和一束探测光同时驱动光力系统时，透射场中将会出现一个额外的FWM光场。这一现象也在一些光力系统中得到了研究，如：在复合光力系统中发现两能级系统可以显著地改变空腔的输出场，从而增强FWM强度[38]；在复合原子光力系统中研究了FWM，并发现光腔与原子系综的耦合会使得FWM信号显著增强[39]。

旋转光腔已逐渐成为光力系统研究的热点。在最近的一次实验中，Maayani等[49]利用旋转光腔实现了隔离度达到99.6%的非互易光传输，发现光腔处于顺时针或逆时针旋转模式时都将经历Sagnac效应，故光从一侧进入系统时会发生共振吸收，从另一侧进入系统时几乎是100%透射。随后，复合旋转光力系统也得到了广泛研究。Li等[50]在由光学腔和旋转光腔组成的复合光力系统中研究了如何通过非常规光子阻塞(UPB)实现量子非互易，并发现即使在单光子非线性非常弱的条件下，该系统也会发生非互易UPB。Mirza等[51]研究了使用泵浦探头驱动激光器耦合旋转光腔的光传输特性，并通过控制两个旋转腔的旋转方向相同或相反来改变因Sagnac效应产生的额外光频移大小，研究了如何产生非往复和延迟的探测光传输。Li等[52]在旋转腔光力系统中研究了光机械诱导的二阶边带生成，发现光腔旋转诱导产生的Sagnac效应会导致反循环模式的共振频率分裂，从而使得二阶边带在一个方向上得到增强的同时在另一个方向上被抑制。Chen[53]在光力诱导透明的情况下研究了旋转腔光力系统中光学输出场的性质，通过调整相干声呐泵浦的相位和振幅实现了探测输出场的大正负群延迟，并通过操纵光腔的旋转方向、泵浦场的功率和声子泵浦的相位与振幅实现了缓慢光和快速光之间的可调转换。Li等[54]以旋转非线性光腔实现了光学孤子的非互易控制，发现在旋转的Kerr球形腔中不同方向的输入场会引起不同的孤子状态，还发现通过调整系统参数，可以实现孤子数的定向切换。由此可见，旋转腔在

收稿日期：2022-05-05；**修回日期**：2022-06-13；**录用日期**：2022-06-20；**网络首发日期**：2022-06-30

基金项目：国家自然科学基金(11647001，11804004)、中国博士后科学基金(2020M681973)、安徽省自然科学基金(1708085QA11)、高校优秀青年骨干教师国外访问研修项目(gxgwfx2021024)

通信作者：*chenphysics@126.com

光力系统中的研究取得了重大的进展。然而，很少有研究者关注旋转腔光力系统中光学双稳态和FWM这两个光学非线性现象。

因此，在上述研究的启发下，本文以旋转环形腔为基础研究了复合旋转光力系统中的两个非线性现象。首先，研究了该系统中的光学双稳态行为，发现在Sagnac频移存在的情况下，通过改变环形腔的旋转模式或旋转速率可以灵活地控制光学双稳态。然后，同时用频率为ω_{p}的较强泵浦场和频率为ω_{L}的较弱信号光来驱动该旋转腔，发现透射场中出现了FWM光场，并且环形腔的旋转模式或旋转速率对FWM谱有较大的影响。最后，探讨了施加额外声子泵浦对系统FWM的影响，发现当施加一个微小的外力时，系统的FWM谱线会发生显著变化。

2　模型和理论

系统模型如图1所示，这是与固定锥形光纤耦合的复合旋转环形腔光力系统，该系统中的环形腔由与其下方相连的旋转装置以角速度Ω带动。输入系统的驱动光总是从光纤左侧进入并以顺时针方向在光腔内传播。在此规定：环形腔沿着顺时针旋转为正旋转，记为$\Omega>0$；环形腔沿着逆时针旋转为逆旋转，记为$\Omega<0$。可以看出，环形腔既可以正旋转，也可以逆旋转，环形腔的腔频为ω_{a}，本征损耗为$\gamma_{\mathrm{a}}=\omega_{\mathrm{a}}/Q$（$Q$为环形腔的光学品质因子），由频率为$\omega_{\mathrm{p}}$的较强泵浦场和频率为$\omega_{\mathrm{L}}$的较弱信号光驱动。耦合到环形腔中的光因受到辐射压力产生了机械模式（声学模式）。该声学模式由一个额外声子泵浦驱动，该泵浦的振幅为F_{m}、频率为ω_{q}和相位为φ_{m}。该旋转腔以角速度Ω旋转，由于Sagnac效应的存在，故在腔中循环的光会产生一个Sagnac频移[55-56]，即

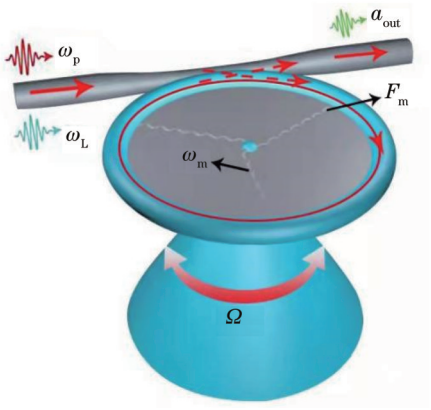

图1　复合旋转光力系统示意图

Fig. 1　Schematic diagram of hybrid spinning optomechanical system

$$\omega_{\mathrm{a}}\rightarrow\omega_{\mathrm{a}}+\Delta_{\mathrm{sag}},\tag{1}$$

$$\Delta_{\mathrm{sag}}=\pm\frac{nr\Omega\omega_{\mathrm{a}}}{c}\left(1-\frac{1}{n^2}-\frac{\lambda}{n}\cdot\frac{\mathrm{d}n}{\mathrm{d}\lambda}\right),\tag{2}$$

式中：n和r分别为折射率和环形腔的半径；λ为光学模式的波长；c为真空中的光速；Δ_{sag}为Sagnac效应引起的光频移；$\mathrm{d}n/\mathrm{d}\lambda$为色散项，它描述了Sagnac效应的起源[49,56]，其数值相当小，约为1%。

对系统作相对于泵浦频率ω_{p}的旋转波变换，变换后旋转环形腔光力系统与固定光纤耦合形成的复合旋转光力系统的哈密顿量[57]可以表示为

$$\hat{H}=\hbar\Delta\hat{a}^{\dagger}\hat{a}-\hbar g\hat{x}\hat{a}^{\dagger}\hat{a}+\frac{\hat{p}^2}{2m}+\frac{1}{2}m\omega_{\mathrm{m}}^2\hat{x}^2+\frac{\hat{p}_{\theta}^2}{2mr^2}+\mathrm{i}\hbar\sqrt{\kappa_{\mathrm{e}}}\,\varepsilon_{\mathrm{p}}\left(\hat{a}^{\dagger}-\hat{a}\right)+\mathrm{i}\hbar\sqrt{\kappa_{\mathrm{e}}}\,\varepsilon_{\mathrm{L}}\left[\hat{a}^{\dagger}\exp\left(-\mathrm{i}\eta t\right)-\hat{a}\exp\left(\mathrm{i}\eta t\right)\right]+2\hat{x}F_{\mathrm{m}}\cos\left(\omega_{\mathrm{q}}t+\varphi_{\mathrm{m}}\right),\tag{3}$$

式中：$\Delta=\Delta_{\mathrm{a}}\pm\Delta_{\mathrm{sag}}$，其中$\Delta_{\mathrm{a}}=\omega_{\mathrm{a}}-\omega_{\mathrm{p}}$为腔频与泵浦频率的失谐；$g=\omega_{\mathrm{a}}/r$为系统光力耦合强度；$\hat{x}$、$\hat{p}$分别为环形腔的位移算符和动量算符，且满足对易条件$\left[\hat{x},\hat{p}\right]=\mathrm{i}$；$\hat{\theta}$、$\hat{p}_{\theta}$分别为环形腔的旋转角度算符和角动量算符，且也满足对易关系$\left[\hat{\theta},\hat{p}_{\theta}\right]=\mathrm{i}$[58]；$\eta$为探测光场与泵浦光场之间的失谐；$\omega_{\mathrm{m}}$为机械模式的频率；$m$为机械振子的有效质量；$\hat{a}^{\dagger}$为环形腔场的二次量子化产生算符；$\hat{a}$为环形腔场的二次量子化湮灭算符；$\kappa_{\mathrm{e}}$为环形腔与光纤耦合的损耗率；$\varepsilon_{\mathrm{p}}=\sqrt{p/\left(\hbar\omega_{\mathrm{p}}\right)}$和$\varepsilon_{\mathrm{L}}=\sqrt{p_{\mathrm{L}}/\left(\hbar\omega_{\mathrm{L}}\right)}$分别为泵浦光的振幅和探测光的振幅，其中$p$为泵浦光功率，$p_{\mathrm{L}}$为探测光功率。式(3)中右侧第1项为腔模的哈密顿量，第2项为环形腔场与机械振子之间的相互作用项，第3、4项为机械模式的哈密顿量，第5项为转动动能，第6项为环形腔场与泵浦光场之间的相互作用，第7项为环形腔场与探测光场之间的相互作用，最后一项为声学模式被额外声子驱动所引起的项。

通过Heisenberg运动方程可以求得算符随时间演化的方程[58-59]，即

$$\dot{\hat{a}}=-\left(\mathrm{i}\Delta-\mathrm{i}g\hat{x}+\beta\right)\hat{a}+\sqrt{\kappa_{\mathrm{e}}}\,\varepsilon_{\mathrm{p}}+\sqrt{\kappa_{\mathrm{e}}}\,\varepsilon_{\mathrm{L}}\exp\left(-\mathrm{i}\eta t\right),\tag{4}$$

$$\ddot{\hat{x}}+\gamma_{\mathrm{m}}\dot{\hat{x}}+\omega_{\mathrm{m}}^2\hat{x}=\frac{g}{m}\hat{a}^{\dagger}\hat{a}+\frac{\hat{p}_{\theta}^2}{m^2r^3}-\frac{2F_{\mathrm{m}}}{m}\cos\left(\omega_{\mathrm{q}}t+\varphi_{\mathrm{m}}\right),\tag{5}$$

$$\dot{\hat{\theta}}=\frac{\hat{p}_{\theta}}{mr^2},\ \dot{\hat{p}}_{\theta}=0,\tag{6}$$

式中：γ_{m}为环形腔中振子的衰减率；$\beta=(\kappa_{\mathrm{e}}+\kappa_{\mathrm{a}})/2$为环形腔模的衰减率，其中$\kappa_{\mathrm{a}}$为环形腔的本征损耗。

为了求解式(4)～(6),对算符进行变换

$$\hat{a}=\bar{\hat{a}}+\hat{a}_{+}\exp(-\mathrm{i}\eta t)+\hat{a}_{-}\exp(\mathrm{i}\eta t),\tag{7}$$

$$\hat{x}=\bar{\hat{x}}+\hat{x}_{+}\exp(-\mathrm{i}\eta t)+\hat{x}_{-}\exp(\mathrm{i}\eta t),\tag{8}$$

式中:$\bar{\hat{a}}$为$\hat{a}$的稳态平均值;$\bar{\hat{x}}$为$\hat{x}$的稳态平均值;$\hat{a}_{+}$、$\hat{a}_{-}$、$\hat{x}_{+}$和$\hat{x}_{-}$类比于原子系统或半导体材料中的非线性极化特征,$\hat{a}_{+}$和$\hat{x}_{+}$为一阶非线性极化项,$\hat{a}_{-}$和$\hat{x}_{-}$为三阶非线性极化项。将式(7)和式(8)代入式(4)～(6)中,可以得到稳态平均值方程组,即

$$\bar{\hat{a}}=\frac{\sqrt{\kappa_{\mathrm{e}}}\,\varepsilon_{\mathrm{p}}}{\beta+\mathrm{i}\Delta-\mathrm{i}g\bar{\hat{x}}},\tag{9}$$

$$\bar{\hat{x}}=\frac{\kappa_{\mathrm{e}}g\left|\bar{\hat{a}}\right|^{2}}{m\omega_{\mathrm{m}}^{2}\left[\beta^{2}+\left(\Delta-g\bar{\hat{x}}\right)^{2}\right]}+r\left(\frac{\Omega}{\omega_{\mathrm{m}}}\right)^{2},\tag{10}$$

从式(9)和式(10)中很明显看出机械位移$\bar{\hat{x}}$和环形腔内光子数$\left|\bar{\hat{a}}\right|^{2}$强烈依赖于系统中环形腔的转速$\Omega$和Sagnac频移$\Delta_{\mathrm{sag}}$,这两个数值大小都会影响该光力系统的双稳态行为。将式(9)和式(10)联立并令腔内光子数为$n_{\mathrm{c}}=\left|\bar{\hat{a}}\right|^{2}$,得出环形腔内光子数与泵浦光的关系为

$$n_{\mathrm{c}}\left\{\beta^{2}+\Delta^{2}+g^{2}\left[\frac{g}{m\omega_{\mathrm{m}}^{2}}n_{\mathrm{c}}+r\left(\frac{\Omega}{\omega_{\mathrm{m}}}\right)^{2}\right]^{2}-2\Delta g\left[\frac{g}{m\omega_{\mathrm{m}}^{2}}n_{\mathrm{c}}+r\left(\frac{\Omega}{\omega_{\mathrm{m}}}\right)^{2}\right]\right\}=\kappa_{\mathrm{e}}\varepsilon_{\mathrm{p}}^{2},\tag{11}$$

再将式(7)和式(8)式代入式(4)～(6)中,略去二阶和高阶小量,并令$\eta=\omega_{\mathrm{L}}-\omega_{\mathrm{p}}$,$\omega_{\mathrm{q}}=\omega_{\mathrm{L}}-\omega_{\mathrm{p}}$,化简并比较方程两边$\exp(\mathrm{i}\eta t)$项可求解得到

$$\hat{a}_{-}=\frac{\mathrm{i}g^{2}\bar{\hat{a}}^{2}\sqrt{\kappa_{\mathrm{e}}}\,\varepsilon_{\mathrm{p}}B-g^{3}\left|\bar{\hat{a}}\right|^{2}\bar{\hat{a}}F_{\mathrm{m}}\exp(\mathrm{i}\varphi_{\mathrm{m}})-\mathrm{i}g\bar{\hat{a}}F_{\mathrm{m}}\exp(\mathrm{i}\varphi_{\mathrm{m}})\left(A_{1}B+\mathrm{i}g^{2}\left|\bar{\hat{a}}\right|^{2}\right)}{\left(A_{2}B-\mathrm{i}g^{2}\left|\bar{\hat{a}}\right|^{2}\right)\left(A_{1}B+\mathrm{i}g^{2}\left|\bar{\hat{a}}\right|^{2}\right)-g^{4}\left|\bar{\hat{a}}\right|^{4}},\tag{12}$$

式中:$A_{1}=\beta-\mathrm{i}\Delta+\mathrm{i}g\bar{\hat{x}}+\mathrm{i}\eta$;$A_{2}=\beta+\mathrm{i}\Delta-\mathrm{i}g\bar{\hat{x}}+\mathrm{i}\eta$;$B=m\left(\omega_{\mathrm{m}}^{2}-\eta^{2}+\mathrm{i}\gamma_{\mathrm{m}}\eta\right)$。

利用输入-输出关系$\hat{a}_{\mathrm{out}}(t)=\hat{a}_{\mathrm{in}}(t)-\sqrt{\kappa_{\mathrm{e}}}\,\hat{a}(t)$,其中$\hat{a}_{\mathrm{out}}(t)$为输出场算符,$\hat{a}_{\mathrm{in}}(t)$为输入场算符,得到

$$\begin{aligned}\left\langle\hat{a}_{\mathrm{out}}(t)\right\rangle&=\left(\varepsilon_{\mathrm{p}}-\sqrt{\kappa_{\mathrm{e}}}\,a_{0}\right)\exp(-\mathrm{i}\omega_{\mathrm{p}}t)+\left(\varepsilon_{\mathrm{L}}-\sqrt{\kappa_{\mathrm{e}}}\,\hat{a}_{+}\right)\exp\left[-\mathrm{i}\left(\eta+\omega_{\mathrm{p}}\right)t\right]-\sqrt{\kappa_{\mathrm{e}}}\,\hat{a}_{-}\exp\left[-\mathrm{i}\left(\eta-\omega_{\mathrm{p}}\right)t\right]=\\&\left(\varepsilon_{\mathrm{p}}-\sqrt{\kappa_{\mathrm{e}}}\,a_{0}\right)\exp(-\mathrm{i}\omega_{\mathrm{p}}t)+\left(\varepsilon_{\mathrm{L}}-\sqrt{\kappa_{\mathrm{e}}}\,\hat{a}_{+}\right)\exp(-\mathrm{i}\omega_{\mathrm{L}}t)-\sqrt{\kappa_{\mathrm{e}}}\,\hat{a}_{-}\exp\left[-\mathrm{i}\left(2\omega_{\mathrm{p}}-\omega_{\mathrm{L}}\right)t\right],\end{aligned}\tag{13}$$

式中:a_{0}为环形腔场的定态解。式(13)右边包含三个部分,分别为泵浦频率ω_{p}产生的驱动场、探测频率ω_{L}产生的探测场(反斯托克斯场)和频率为$2\omega_{\mathrm{p}}-\omega_{\mathrm{L}}$的FWM场(斯托克斯场)[36]。系统FWM场的强度可定义为

$$I_{\mathrm{FWM}}=\left|\frac{\sqrt{\kappa_{\mathrm{e}}}\,\hat{a}_{-}}{\varepsilon_{\mathrm{L}}}\right|。\tag{14}$$

3　分析与讨论

本文利用现有的实验数据分两部分来研究该复合旋转系统中的非线性行为。设定参数[59]:$m=2\ \mu\mathrm{g}$,$n=1.44$,$Q=3\times10^{7}$,$r=0.25\ \mathrm{mm}$,$\lambda=1.55\ \mu\mathrm{m}$,$\kappa_{\mathrm{e}}=\kappa_{\mathrm{a}}=\omega_{\mathrm{a}}/Q$,$p=10\ \mathrm{W}$,$\Delta_{\mathrm{a}}=0$,$\omega_{\mathrm{m}}=200\ \mathrm{MHz}$,$\gamma_{\mathrm{m}}=0.2\ \mathrm{MHz}$。

3.1　光学双稳态

式(11)可看作复合旋转光力系统中环形腔腔内光子数n_{c}与泵浦光功率p的一元三次方程,此方程可描述该系统的光学双稳态行为。为了分析不同旋转方向对系统双稳态行为的影响,图2给出了环形腔在正旋转、不旋转、逆旋转情况下腔内光子数随泵浦功率p的变化情况。可以看出:三条曲线的腔内光子数最初都处于较低的稳定分支(对应于最小的实根);当输入的泵浦功率逐渐增加时,腔内光子数首先在下稳定分支增加,当它到达下分支的末端时即第一个临界值时,它就会跳转到上稳定分支,即输入泵浦功率的增加会导致环形腔内光子数的增加;来到上稳定分支后,当输入泵浦功率降低时,腔内光子数开始下降,但仍在上稳定分支曲线上变化;当泵浦功率降低到腔内光子数达到第二个临界值时,它就会来到下稳定分支。此外,对比图2这三条曲线可知,当$\Omega=-10\ \mathrm{kHz}$时,观察光学双稳态所需的泵浦功率相对较低,$\Omega=0$时次之,而$\Omega=10\ \mathrm{kHz}$时观察光学双稳态所需的泵浦功率最高。同时,在泵浦驱动功率更高的情况下,正旋转时双稳态曲线的上稳定分支大于腔静止的情况,逆旋转时相对最低。因此,改变环形腔的旋转方向可有效操控系统的光学双稳态行为。

同样地,为了分析环形腔的旋转速率大小对系统光学双稳态行为的影响。图3(a)、(b)分别给出了不同正旋转速率和不同逆旋转速率下腔内光子数n_{c}随泵浦功率p的变化情况。从图3(a)可知:当环形腔正旋转时,随着旋转速率的增大,观察光学双稳态所需的泵浦功率相对较大;在泵浦驱动功率较大的情况下,当正旋转速率增大时,所对应的双稳态曲线的上稳定分支也在增大。从图3(b)可知:随着环形腔逆旋转速率的增大,观察光学双稳定所需的泵浦功率相对较低;双稳

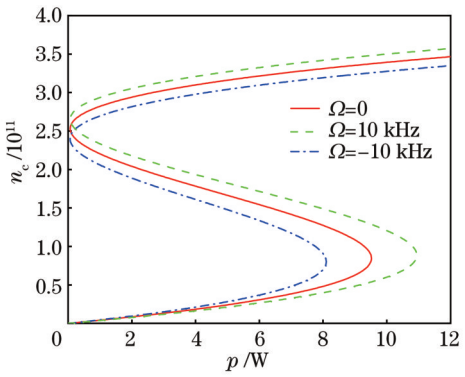

图 2　在三个不同旋转方向下腔内光子数n_c随泵浦功率p的变化

Fig. 2　Intracavity photon number n_c varying with pump power p under three different spinning directions

态曲线的上稳定分支会随着逆旋转速率的增大而减小。

图 2 和图 3 中现象的物理本质可解释为：当同时用泵浦光和探测光驱动该复合旋转光力系统时，腔内产生的辐射压力在拍频η处共振相干，这会诱导该光力系统中机械振子在共振处发生振动，进而诱导出斯托克斯散射光（$\omega_S=\omega_p-\omega_a$）和反斯托克斯散射光（$\omega_{AS}=\omega_p+\omega_a$），这两束散射光将在系统中重新建立腔场，诱导光学双稳态产生。然而，复合旋转光力系统中环形腔旋转方向的改变和旋转速率的变化都会产生 Sagnac 频移，导致腔的共振频率Δ发生移动。伴随环形腔共振频率的移动，腔内光子数的双稳态行为将会受到调节：当环形腔正旋转时，腔的共振频率红移，有$\omega_a\rightarrow\omega_a-\left|\Delta_{sag}\right|$；当环形腔逆旋转时，腔的共振频率蓝移，有$\omega_a\rightarrow\omega_a+\left|\Delta_{sag}\right|$。因此，通过改变系统环形腔的旋转方向和调节其旋转速率大小都能有效操控光学双稳态行为。

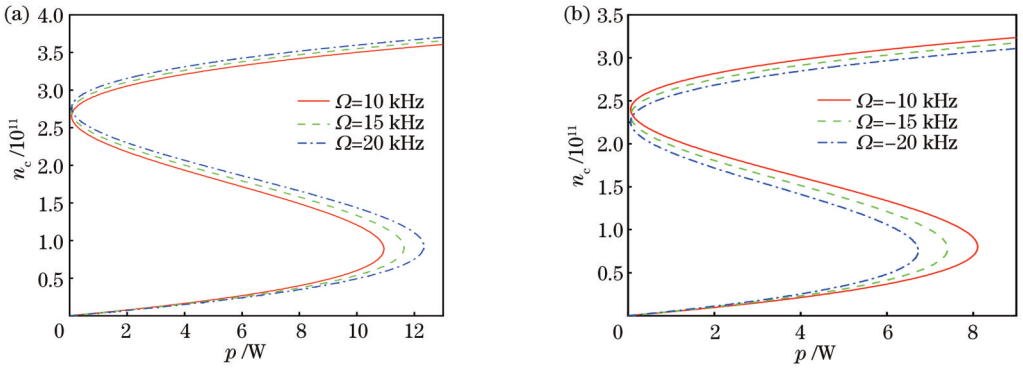

图 3　两种旋转方向下腔内光子数n_c随泵浦功率p的变化情况。(a) $\Omega>0$；(b) $\Omega<0$

Fig. 3　Intracavity photon number n_c varying with pump power p under two spinning directions. (a) $\Omega>0$; (b) $\Omega<0$

3.2　四波混频

在研究了复合旋转光力系统中光学双稳态行为的基础上，对腔光力系统中另外一种典型的非线性行为（FWM 现象）进行了研究。首先，研究了无外力F_m下腔不同旋转模式对系统 FWM 的影响，通过联立式(12)和式(14)，在图 4 中给出了环形腔在三种旋转状态下系统 FWM 强度随探测场-环形腔场失谐$\Delta_s=\omega_L-\omega_a$的变化情况。从图 4(a)可以发现，当$\Omega=0$时，FWM 强度谱中$\Delta_s=\pm200$ MHz 处出现两个对称峰，在$\Delta_s=0$附近出现模式分裂现象。从图 4(b)可以发现，当$\Omega=10$ kHz 时，FWM 强度谱中$\Delta_s=\pm200$ MHz 处的峰值增大，在$\Delta_s=0$ 附近的模式分裂消失且变成一个尖峰。然而，从图 4(c)可以发现，当$\Omega=-10$ kHz 时，$\Delta_s=\pm200$ MHz 处的峰值减小，并可以观察到$\Delta_s=0$附近的模式分裂愈加明显。

为了分析不同旋转速率对该系统中 FWM 强度的影响，图 5 给出了正旋转、逆旋转模式下不同旋转速率的 FWM 强度随探测场-环形腔场失谐Δ_s的变化情况。对比图 4(a)、(b)可以发现，当腔旋转速率从$\Omega=0$增大到$\Omega=10$ kHz 时，$\Delta_s=\pm200$ MHz 处的峰值增大且$\Delta_s=0$附近的模式分裂消失。然而，图 5(a)～(c)显示：当腔的旋转速率由 10 kHz 增大到 15 kHz 时，在$\Delta_s=\pm200$ MHz 处的 FWM 强度减弱，且在$\Delta_s=0$ 附近出现微弱的模式分裂；当继续增大腔的旋转速率到 20 kHz 时，$\Delta_s=0$ 附近处出现明显的模式分裂。由此可以发现，$\Omega=10$ kHz 是腔正旋转时区分共振处是否发生模式分裂的临界值。由图 5(e)～(f)可知，随着腔的旋转速率由 −10 kHz 增大至 −20 kHz 时，$\Delta_s=\pm200$ MHz 处的 FWM 峰值在减小，并且$\Delta_s=0$ 附近的模式分裂现象愈加强烈，这说明当腔逆旋转速率增大时，系统的 FWM 强度会减弱，并且减弱的这部分能量会被系统共振处的模式分裂所消耗。

此外，进一步研究了施加外力F_m对系统的 FWM 谱的影响，图 6 给出了环形腔在$\Omega=10$ kHz 和$\Omega=-10$ kHz 条件下施加不同外力F_m时 FWM 强度随探测场-环形腔场失谐Δ_s的变化情况。由图 4(b)可知，当腔正旋转且不受外力F_m时，在系统 FWM 强度谱中$\Delta_s=\pm200$ MHz 处存在两个对称的峰，且$\Delta_s=0$ 附近没有出现模式分裂。当施加外力F_m时，从图 6(a)～(c)可以清晰看到，在 FWM 强度谱中$\Delta_s=\pm200$ MHz

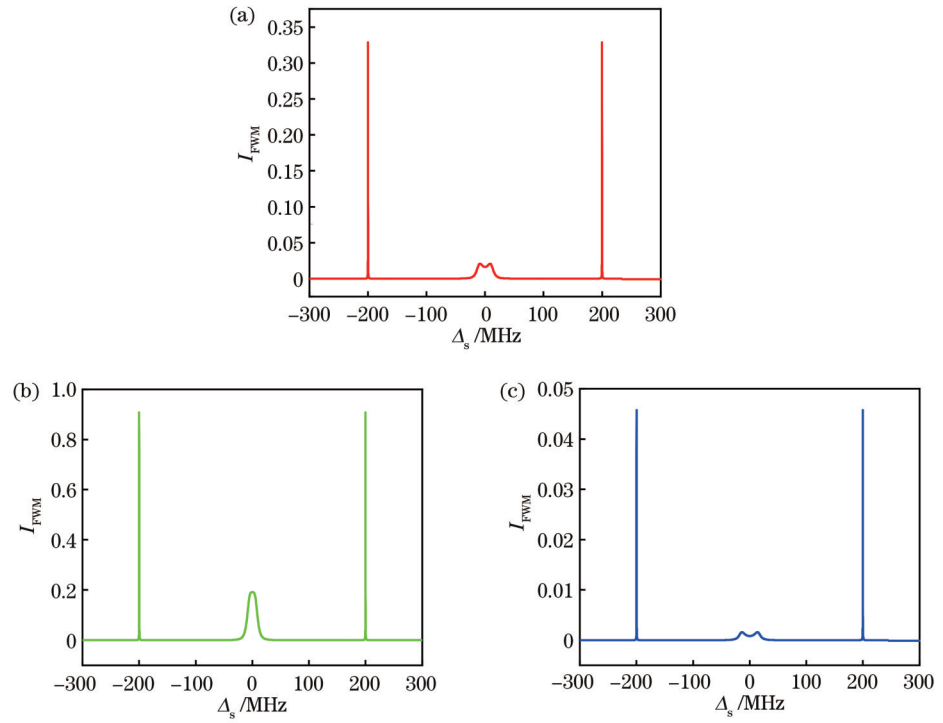

图 4　三个不同旋转方向下 I_{FWM} 随 Δ_s 的变化情况。(a) $\Omega=0$;(b) $\Omega=10$ kHz;(c) $\Omega=-10$ kHz

Fig. 4　I_{FWM} varying with Δ_s under three different spinning directions. (a) $\Omega=0$; (b) $\Omega=10$ kHz; (c) $\Omega=-10$ kHz

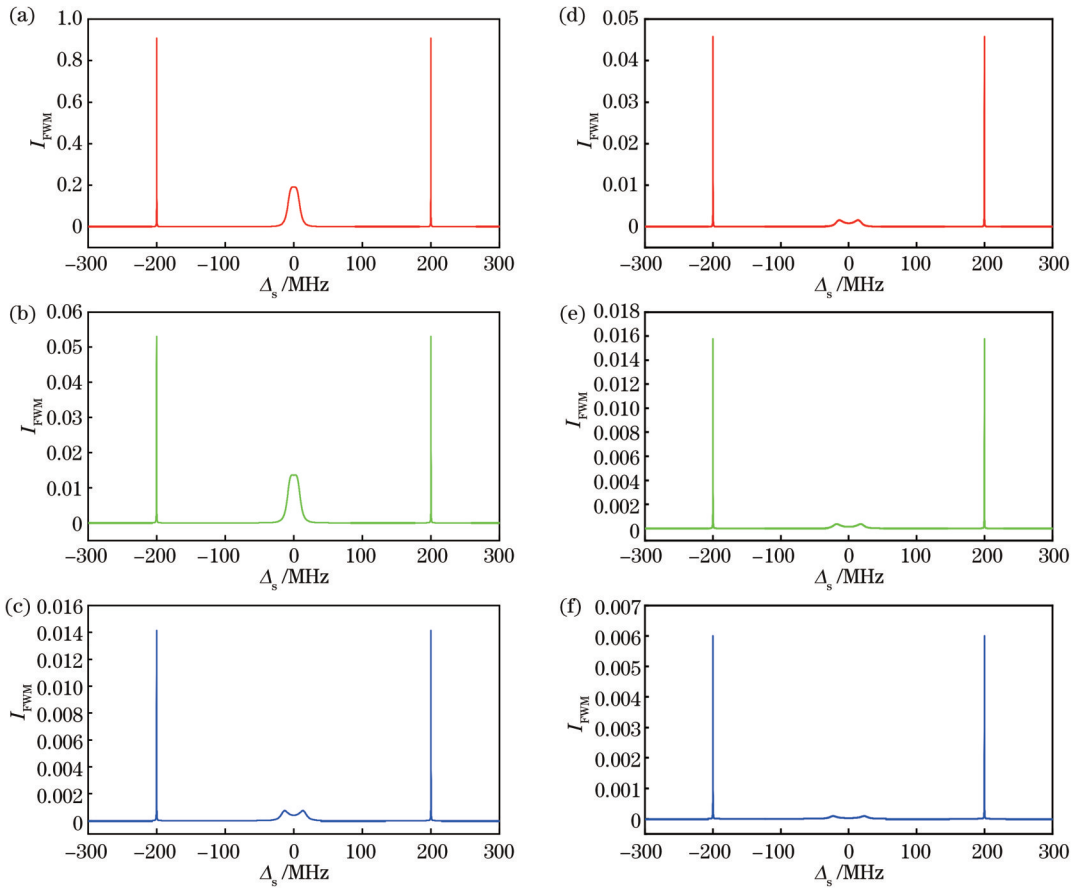

图 5　当 $F_m=0$ 时,不同旋转速率下 I_{FWM} 随 Δ_s 的变化情况。(a) $\Omega=10$ kHz;(b) $\Omega=15$ kHz;(c) $\Omega=20$ kHz;(d) $\Omega=-10$ kHz;(e) $\Omega=-15$ kHz;(f) $\Omega=-20$ kHz

Fig. 5　I_{FWM} varying with Δ_s under different spinning rates when $F_m=0$. (a) $\Omega=10$ kHz; (b) $\Omega=15$ kHz; (c) $\Omega=20$ kHz; (d) $\Omega=-10$ kHz; (e) $\Omega=-15$ kHz; (f) $\Omega=-20$ kHz

处的峰变为左低右高的两个峰，并且峰值随着 F_m 的增大而显著增大，而 $\Delta_s=0$ 附近的峰的峰值随着外力 F_m 的增大在减小。由图 4(c)可知，当腔逆旋转且不受外力 F_m 时，在系统 FWM 强度谱中 $\Delta_s=\pm200$ MHz 处存在两个对称的峰，且 $\Delta_s=0$ 附近出现模式分裂。当施加外力 F_m 时，从图 6(d)～(f)可以发现，在 FWM 强度谱中 $\Delta_s=\pm200$ MHz 处的峰变为左高右低的两个峰，并且峰值也随着外力 F_m 的增大而增大，在 $\Delta_s=0$ 附近的模式分裂逐渐消失。由图 6 可以发现：当外力 F_m 存在时，不论腔处于正旋转模式还是逆旋转模式，系统的 FWM 强度都会比无外力 F_m 时强；正旋转情况下对系统施加额外声子泵浦驱动可以获得较高的 FWM 强度。

同样地，为了分析施加同一外力 F_m 时不同旋转速率对系统 FWM 谱的影响，图 7 给出了两种旋转模式下，外力 $F_m=0.1$ fN 时不同速率所对应的 FWM 强度随探测场-环形腔场失谐 Δ_s 的变化情况。由图 7 可知，同一外力 F_m 下无论腔处于哪种旋转模式，增大旋转速率都会使 $\Delta_s=\pm200$ MHz 处的两个峰的峰值减小，且减小的能量会被用于共振处的模式分裂。

图 4～7 中现象的物理本质可解释为：输入系统中的泵浦光和探测光与机械振动模式通过环形腔相互作用从而产生量子相干效应。当探测光与泵浦光之间的失谐 $\eta=\omega_L-\omega_p$ 相接近时，系统机械振子开始振动并产生斯托克斯散射光（$\omega_S=\omega_p-\omega_a$），这一过程中电子在斯托克斯散射光频率附近吸收两个光子，放出一个光子，诱导 FWM 产生。复合旋转光力系统中环形腔的旋转方向改变和旋转速率改变都会产生 Sagnac 频移，从而导致腔的共振频率 Δ 发生移动：当环形腔正旋转时，腔的共振频率红移，有 $\omega_a\rightarrow\omega_a-\left|\Delta_{sag}\right|$，FWM 强度增大且共振处模式分裂消失；当环形腔逆旋转时，腔的共振频率蓝移，有 $\omega_a\rightarrow\omega_a+\left|\Delta_{sag}\right|$，FWM 强度减小且共振处模式分裂加剧。

光学双稳态和 FWM 这两个典型光学非线性现象在之前就有较多研究者关注。Chen 等[20]在复合光子-分子光力系统中对光学双稳态和 FWM 展开了研究，其中光子-分子腔由两个耳语画廊模式微腔组成，分析了两腔之间的耦合强度、两个腔体的衰减率比，以及泵浦功率对光学双稳态和 FWM 谱的影响。Chen 等[21]研究了原子-腔-镜耦合的三模光力系统中腔泵失谐、泵浦功率、原子泵失谐和原子-腔耦合强度对系统光学双稳态行为的影响。Jiang 等[36]在由两腔耦合一个公共机械振子的双模光力系统中对 FWM 展开了研究，

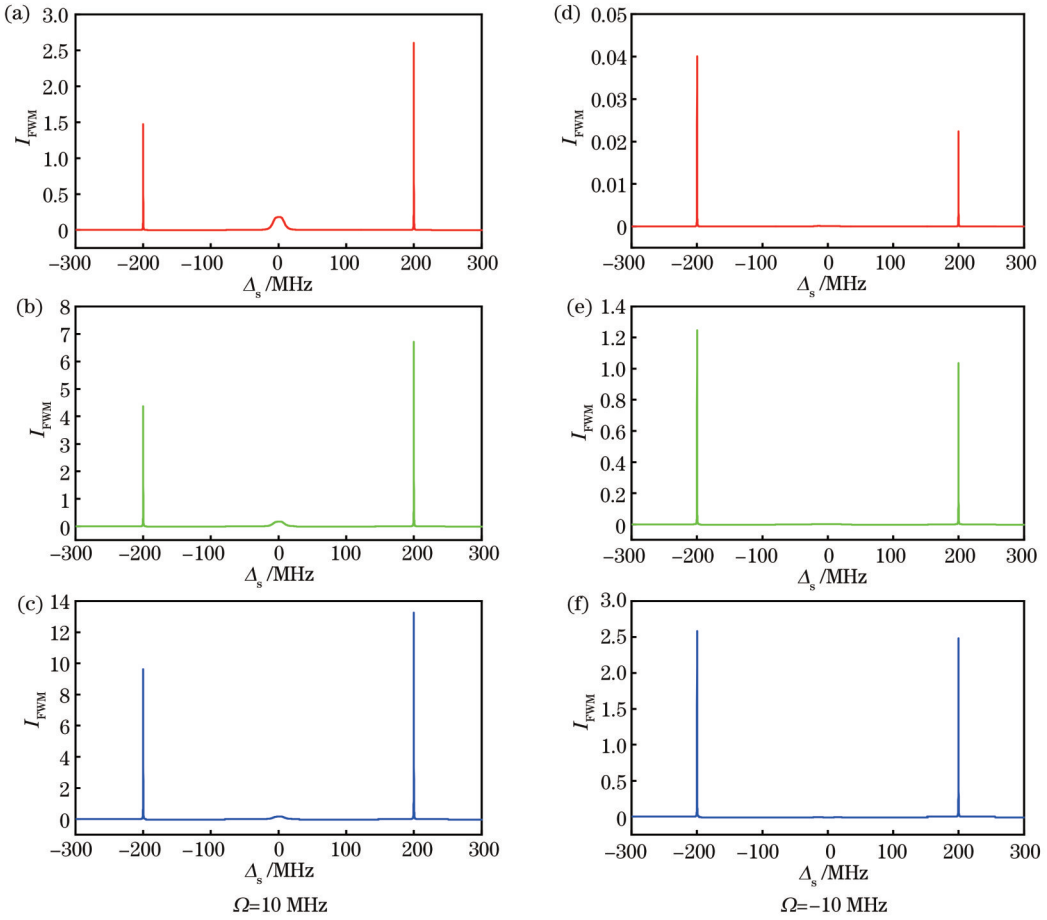

图 6　不同外力下 I_{FWM} 随 Δ_s 的变化情况。(a)(d) $F_m=0.1$ fN；(b)(e) $F_m=0.2$ fN；(c)(f) $F_m=0.3$ fN

Fig. 6　I_{FWM} varying with Δ_s under different external forces. (a)(d) $F_m=0.1$ fN; (b)(e) $F_m=0.2$ fN; (c)(f) $F_m=0.3$ fN

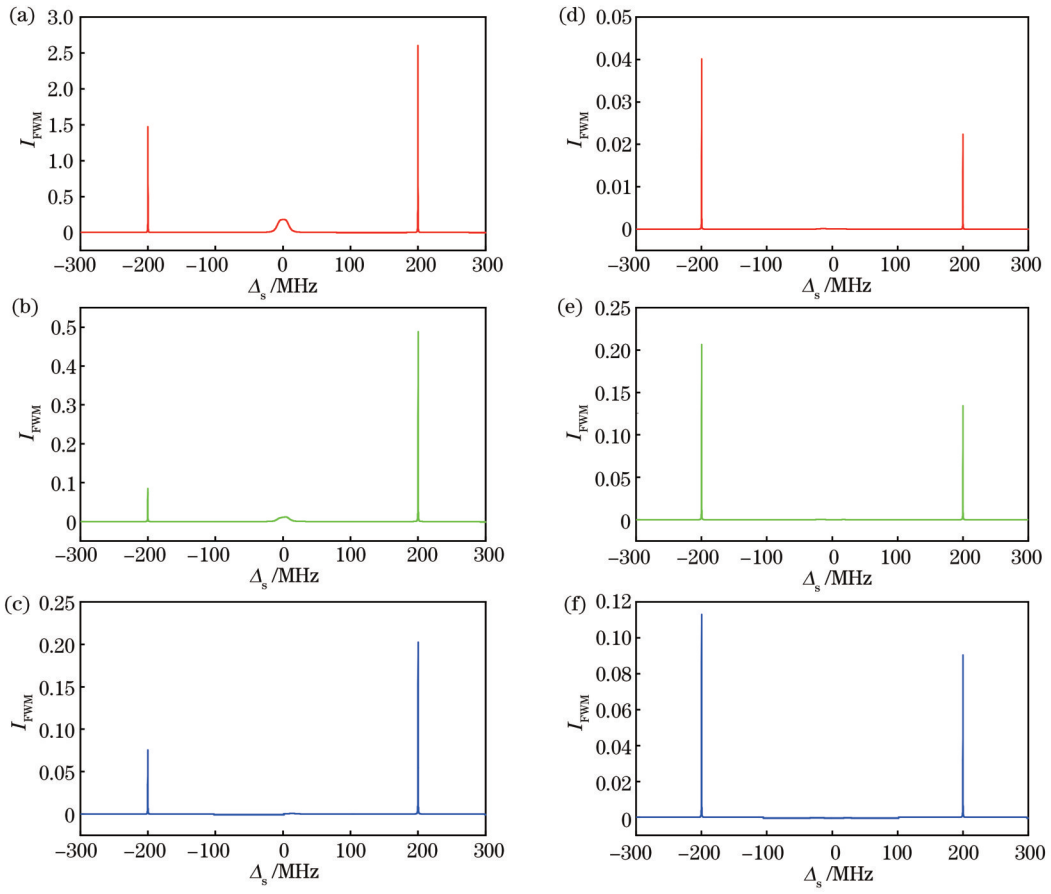

图 7 当 $F_m=0.1$ fN 时，不同旋转速率下 I_{FWM} 随 Δ_s 的变化情况。(a) $\Omega=10$ kHz；(b) $\Omega=15$ kHz；(c) $\Omega=20$ kHz；(d) $\Omega=-10$ kHz；(e) $\Omega=-15$ kHz；(f) $\Omega=-20$ kHz

Fig. 7 I_{FWM} varying with Δ_s under different spinning rates when $F_m=0.1$ fN. (a) $\Omega=10$ kHz; (b) $\Omega=15$ kHz; (c) $\Omega=20$ kHz; (d) $\Omega=-10$ kHz; (e) $\Omega=-15$ kHz; (f) $\Omega=-20$ kHz

讨论了两腔在不同边带被驱动时FWM强度的变化。Jiang等[38]采用的是由机械振子同时耦合腔场和两级系统(量子位)所组成的复合光力系统，使用强控制场驱动控制稳态光子数、声子数和总体反演的双稳态行为，分析了量子比特-谐振器耦合强度对双稳态行为和FWM强度的影响。然而，本文是在复合旋转光力系统中围绕旋转腔对光学双稳态和FWM展开研究的，不同模式、不同旋转速率下的光腔都将发生Sagnac效应，进而对其光学特性产生影响。同时，本文进一步研究了施加额外声子泵浦于系统的机械模式对FWM强度的影响。

4 结 论

研究了复合旋转光力系统中两个典型的光学非线性行为，即光学双稳态行为和FWM现象。研究了利用一束较强泵浦光和一束较弱探测光同时驱动复合旋转光力系统时，通过控制系统中环形腔的旋转方向和旋转速率大小都可实现对该系统光学双稳态行为的有效调控。同时，研究了有效腔-泵浦光在共振条件下系统的FWM现象。对比静止状态下系统的FWM强度发现：当环形腔正旋转时，系统会将共振处模式分裂的能量用于增加FWM强度谱中尖峰的峰值；当环形腔逆旋转时，系统会消耗FWM强度来增强模式分裂行为。不仅如此，无论系统是正旋转还是逆旋转，当旋转速率增加时，系统都会消耗FWM场的强度来增强模式分裂行为。此外，进一步研究了在该复合旋转光力系统中对机械模式施加微小外力时FWM现象的变化，发现：有外力时FWM谱的对称性会被破坏，呈现出正旋转时左低右高和逆旋转时左高右低的现象；不论在哪种旋转模式下，同一速率下外力的增加都会使FWM谱的峰值显著增大；当施加同一外力时，正旋转速率或逆旋转速率的增大都会降低系统的FWM强度。本研究在量子信息网络中有潜在的应用前景。

参 考 文 献

[1] Aspelmeyer M, Kippenberg T J, Marquardt F. Cavity optomechanics[J]. Reviews of Modern Physics, 2014, 86(4): 1391.

[2] Metcalfe M. Applications of cavity optomechanics[J]. Applied Physics Reviews, 2014, 1(3): 031105.

[3] Schliesser A, Arcizet O, Rivière R, et al. Resolved-sideband cooling and position measurement of a micromechanical oscillator close to the Heisenberg uncertainty limit[J]. Nature Physics, 2009, 5(7): 509-514.

[4] Basiri-Esfahani S, Akram U, Milburn G J. Phonon number measurements using single photon opto-mechanics[J]. New Journal of Physics, 2012, 14(8): 085017.
[5] Gavartin E, Verlot P, Kippenberg T J. A hybrid on-chip optomechanical transducer for ultrasensitive force measurements [J]. Nature Nanotechnology, 2012, 7(8): 509-514.
[6] Krause A G, Winger M, Blasius T D, et al. A high-resolution microchip optomechanical accelerometer[J]. Nature Photonics, 2012, 6(11): 768-772.
[7] Schreppler S, Spethmann N, Brahms N, et al. Optically measuring force near the standard quantum limit[J]. Science, 2014, 344(6191): 1486-1489.
[8] Xiong H, Si L G, Wu Y. Precision measurement of electrical charges in an optomechanical system beyond linearized dynamics [J]. Applied Physics Letters, 2017, 110(17): 171102.
[9] Matsumoto N, Cataño-Lopez S B, Sugawara M, et al. Demonstration of displacement sensing of a mg-scale pendulum for mm- and mg-scale gravity measurements[J]. Physical Review Letters, 2019, 122(7): 071101.
[10] 喻富, 肖添, 何高倩, 等. 超导量子比特耦合微波腔和机械谐振器系统的探测场吸收特性研究[J]. 激光与光电子学进展, 2022, 59(3): 0327001.
Yu F, Xiao T, He G Q, et al. Probe absorption properties of a superconducting qubit coupled to microwave cavity and mechanical resonator[J]. Laser & Optoelectronics Progress, 2022, 59(3): 0327001.
[11] Schliesser A, Rivière R, Anetsberger G, et al. Resolved-sideband cooling of a micromechanical oscillator[J]. Nature Physics, 2008, 4(5): 415-419.
[12] Teufel J D, Donner T, Li D L, et al. Sideband cooling of micromechanical motion to the quantum ground state[J]. Nature, 2011, 475(7356): 359-363.
[13] Chan J, Alegre T P M, Safavi-Naeini A H, et al. Laser cooling of a nanomechanical oscillator into its quantum ground state[J]. Nature, 2011, 478(7367): 89-92.
[14] Chen X, Liu Y C, Peng P, et al. Cooling of macroscopic mechanical resonators in hybrid atom-optomechanical systems [J]. Physical Review A, 2015, 92(3): 033841.
[15] Lai D G, Zou F, Hou B P, et al. Simultaneous cooling of coupled mechanical resonators in cavity optomechanics[J]. Physical Review A, 2018, 98(2): 023860.
[16] Tian L. Robust photon entanglement via quantum interference in optomechanical interfaces[J]. Physical Review Letters, 2013, 110(23): 233602.
[17] Wang Y D, Clerk A A. Reservoir-engineered entanglement in optomechanical systems[J]. Physical Review Letters, 2013, 110 (25): 253601.
[18] Liao J Q, Law C K. Correlated two-photon scattering in cavity optomechanics[J]. Physical Review A, 2013, 87(4): 043809.
[19] Mirza I M. Strong coupling optical spectra in dipole-dipole interacting optomechanical Tavis-Cummings models[J]. Optics Letters, 2016, 41(11): 2422-2425.
[20] Chen H J, Wu H W, Yang J Y, et al. Controllable optical bistability and four-wave mixing in a photonic-molecule optomechanics[J]. Nanoscale Research Letters, 2019, 14(1): 73.
[21] Chen B, Wang X F, Yan J K, et al. Controllable optical bistability in a three-mode optomechanical system with atom-cavity-mirror couplings[J]. Superlattices and Microstructures, 2018, 113: 301-309.
[22] Wang Z, Jiang C, He Y, et al. Tunable optical bistability in multi-mode optomechanical systems[J]. Journal of the Optical Society of America B, 2020, 37(2): 579-585.
[23] 章建帅, 张红军, 孙辉. 量子相干调控金刚石锡空位色心光学双稳研究[J]. 光学学报, 2020, 40(12): 1219001.
Zhang J S, Zhang H J, Sun H. Controlling optical bistability through quantum coherence in tin-vacancy color centers in diamond[J]. Acta Optica Sinica, 2020, 40(12): 1219001.
[24] Xiong H, Wu Y. Fundamentals and applications of optomechanically induced transparency[J]. Applied Physics Reviews, 2018, 5(3): 031305.
[25] Yang Q, Hou B P, Lai D G. Local modulation of double optomechanically induced transparency and amplification[J]. Optics Express, 2017, 25(9): 9697-9711.
[26] Mukherjee K, Jana P C. Optically induced transparency in coupled micro-cavities: tunable Fano resonance[J]. The European Physical Journal D, 2019, 73(12): 264.
[27] Qing H, Badshah F, Din R U, et al. Optomechanically induced transparency and the long-lived slow light in a nonlinear system [J]. Journal of the Optical Society of America B, 2018, 35(7): 1649-1657.
[28] 董雅宾, 庞嘉璐, 杨丽, 等. 原子介质中的近共振增益光栅[J]. 中国激光, 2021, 48(3): 0312002.
Dong Y B, Pang J L, Yang L, et al. Nearly-resonant gain grating in atomic media[J]. Chinese Journal of Lasers, 2021, 48 (3): 0312002.
[29] Chen B, Shang L, Wang X F, et al. Atom-assisted second-order sideband generation in an optomechanical system with atom -cavity-resonator coupling[J]. Physical Review A, 2019, 99(6): 063810.
[30] Wang L D, Yan J K, Zhu X F, et al. Tunable second-order sideband effects in a three-mode optomechanical system containing a single quantum well[J]. Physica E, 2017, 89: 134-138.
[31] Liu Z X, Xiong H, Wu Y. Generation and amplification of a high-order sideband induced by two-level atoms in a hybrid optomechanical system[J]. Physical Review A, 2018, 97(1): 013801.
[32] Yang W X, Chen A X, Xie X T, et al. Enhanced generation of higher-order sidebands in a single-quantum-dot-cavity system coupled to a PT-symmetric double cavity[J]. Physical Review A, 2017, 96(1): 013802.
[33] Gu K H, Yan X B, Zhang Y, et al. Tunable slow and fast light in an atom-assisted optomechanical system[J]. Optics Communications, 2015, 338: 569-573.
[34] Jiang C, Jiang L, Yu H L, et al. Fano resonance and slow light in hybrid optomechanics mediated by a two-level system[J]. Physical Review A, 2017, 96(5): 053821.
[35] Jiang C, Cui Y S, Zhai Z Y, et al. Phase-controlled amplification and slow light in a hybrid optomechanical system [J]. Optics Express, 2019, 27(21): 30473-30485.
[36] Jiang C, Cui Y S, Liu H X. Controllable four-wave mixing based on mechanical vibration in two-mode optomechanical systems[J]. Europhysics Letters, 2013, 104(3): 34004.
[37] Liu L W, Gengzang D J, Shi Y Q, et al. Controllable four-wave mixing based on hybrid BEC-optomechanical systems[J]. Acta Physica Polonica A, 2019, 136(3): 444-453.
[38] Jiang L, Yuan X R, Cui Y S, et al. Optical bistability and four-wave mixing in a hybrid optomechanical system[J]. Physics Letters A, 2017, 381(38): 3289-3294.
[39] Wang X F, Chen B. Four-wave mixing response in a hybrid atom-optomechanical system[J]. Journal of the Optical Society of America B, 2019, 36(2): 162-167.
[40] 荆杰泰, 张凯, 刘胜帅. 基于原子系综四波混频过程的量子信息协议[J]. 光学学报, 2022, 42(3): 0327003.
Jing J T, Zhang K, Liu S S. Quantum information protocols based on four-wave mixing process in atomic ensemble[J]. Acta Optica Sinica, 2022, 42(3): 0327003.
[41] Farman F, Bahrampour A R. Effects of optical parametric amplifier pump phase noise on the cooling of optomechanical resonators[J]. Journal of the Optical Society of America B, 2013, 30(7): 1898-1904.
[42] Kumar T, Bhattacherjee A B, ManMohan. Dynamics of a movable micromirror in a nonlinear optical cavity[J]. Physical Review A, 2010, 81(1): 013835.

[43] Dorsel A, McCullen J D, Meystre P, et al. Optical bistability and mirror confinement induced by radiation pressure[J]. Physical Review Letters, 1983, 51(17): 1550-1553.
[44] Sete E A, Eleuch H. Controllable nonlinear effects in an optomechanical resonator containing a quantum well[J]. Physical Review A, 2012, 85(4): 043824.
[45] Chen B, Jiang C, Zhu K D. Slow light in a cavity optomechanical system with a Bose-Einstein condensate[J]. Physical Review A, 2011, 83(5): 055803.
[46] Chen B, Jiang C, Li J J, et al. All-optical transistor based on a cavity optomechanical system with a Bose-Einstein condensate [J]. Physical Review A, 2011, 84(5): 055802.
[47] Yan D, Wang Z H, Ren C N, et al. Duality and bistability in an optomechanical cavity coupled to a Rydberg superatom[J]. Physical Review A, 2015, 91(2): 023813.
[48] Xiong W, Jin D Y, Qiu Y Y, et al. Cross-Kerr effect on an optomechanical system[J]. Physical Review A, 2016, 93(2): 023844.
[49] Maayani S, Dahan R, Kligerman Y, et al. Flying couplers above spinning resonators generate irreversible refraction[J]. Nature, 2018, 558(7711): 569-572.
[50] Li B J, Huang R, Xu X W, et al. Nonreciprocal unconventional photon blockade in a spinning optomechanical system[J]. Photonics Research, 2019, 7(6): 630-641.
[51] Mirza I M, Ge W C, Jing H. Optical nonreciprocity and slow light in coupled spinning optomechanical resonators[J]. Optics Express, 2019, 27(18): 25515-25530.
[52] Li W A, Huang G Y, Chen J P, et al. Nonreciprocal enhancement of optomechanical second-order sidebands in a spinning resonator[J]. Physical Review A, 2020, 102(3): 033526.
[53] Chen H J. Phonon pump enhanced fast and slow light in a spinning optomechanical system[J]. Results in Physics, 2021, 31: 105002.
[54] Li B J, Özdemir Ş K, Xu X W, et al. Nonreciprocal optical solitons in a spinning Kerr resonator[J]. Physical Review A, 2021, 103(5): 053522.
[55] Post E J. Sagnac effect[J]. Reviews of Modern Physics, 1967, 39(2): 475-493.
[56] Malykin G B. The Sagnac effect: correct and incorrect explanations[J]. Physics-Uspekhi, 2000, 43(12): 1229-1252.
[57] Lü H, Jiang Y J, Wang Y Z, et al. Optomechanically induced transparency in a spinning resonator[J]. Photonics Research, 2017, 5(4): 367-371.
[58] Davuluri S, Zhu S Y. Controlling optomechanically induced transparency through rotation[J]. Europhysics Letters, 2015, 112 (6): 64002.
[59] Guo H R, Karpov M, Lucas E, et al. Universal dynamics and deterministic switching of dissipative Kerr solitons in optical microresonators[J]. Nature Physics, 2017, 13(1): 94-102.

Nonlinear Behavior Research Based on Hybrid Spinning Optomechanical System

Chen Yonglei, Chen Huajun*, Liu Yunhe, Xie Baohao

School of Mechanics and Photoelectric Physics, Anhui University of Science and Technology, Huainan 232001, *Anhui, China*

Abstract

Objective Optomechanical systems are a research topic that has been proposed in recent years and has attracted the attention of many researchers. In many optomechanical systems, the radiation pressure-induced optomechanical interactions will lead to phonon modes, which in turn affects the optical properties and then results in remarkable quantum interference effects. Therefore, many important breakthroughs have been achieved in optomechanical systems, such as cooling of mechanical resonators, quantum entanglement, optomechanically induced transparency, optical bistability, four-wave mixing, and so on. The radiation pressure-induced breathing mode oscillations of the boundary of the resonator play a key role in the nonlinear phenomena. However, the possible role of rotation of the resonator itself has not been explored. In a rotating device, an additional phase is accumulated for the propagating light, which is called the optical Sagnac effect. A non-reciprocal optical transmission with an isolation of 99.6% is achieved using a rotating optical cavity in a recent experiment. Subsequently, hybrid spinning optomechanical systems have been extensively studied, and several remarkable phenomena have been founded including nonreciprocal photon blockades, nanoparticle sensing, and slow and fast light. However, optical bistability and four-wave mixing have not yet been explored in hybrid spinning optomechanical systems.

Methods In this paper, a hybrid spinning optomechanical system driven by a probe laser and pump laser is built to study optical bistability and four-wave mixing, and the composition of the system is analyzed and the definition of each parameter is explained. The drive light entering the system enters from the left side of the fiber and travels clockwise through the optical cavity. The clockwise and counterclockwise modes of the optical cavity experience Sagnac-Fizeau shifts. According to the obtained Hamiltonian, the Heisenberg equation of motion, factorization, and other methods are used to solve it, and relational expressions describing optical bistability and four-wave mixing can be established. Finally, the influence of additional phonon pumping on the four-wave mixing of the system is discussed, and it is found that a small

external force is applied, and the four-wave mixing spectral line of the system changes significantly.

Results and Discussions The study shows that different properties of optical bistability and four-wave mixing can be observed in the hybrid spinning optomechanical system under different parameter mechanisms. When the optical cavity rotates clockwise, the pump power required to observe the optical bistability is relatively large with the increase in rotation rate. In the case of large pump drive power, when the positive rotation rate increases, the upper stable branch of the corresponding bistable curve increases. This result is reversed when the optical cavity rotates counterclockwise (Fig. 3). In case of no external force and no rotation, two symmetrical peaks appear in the four-wave mixing spectrum, and the mode splitting phenomenon occurs at the resonance. When the optical cavity rotates clockwise, the peak value of the four-wave mixing spectrum will increase, and the mode splitting phenomenon will disappear. When the optical cavity rotates counterclockwise, the peak value of the four-wave mixing spectrum will decrease, and the mode splitting phenomenon gets obvious (Fig. 4). With the increase of the rotation rate when the optical cavity rotates clockwise, the peak value of the four-wave mixing spectrum will gradually decrease, while the mode splitting phenomenon will emerge. From here, the critical value for distinguishing whether pattern splitting occurs at resonances when the optical cavity rotates clockwise can be determined. With the increase of the rotation rate when the optical cavity rotates counterclockwise, the peak value of the four-wave mixing spectrum will decrease, and the mode splitting phenomenon gets obvious (Fig. 5). In case of a small external force and rotation rate, two symmetrical peaks become asymmetrical. With the increase of the external force when the optical cavity is at a fixed rotation rate, the peak value of the four-wave mixing spectrum will increase significantly, and there is no pattern splitting at the resonance (Fig. 6). However, whether the optical cavity rotates clockwise or counterclockwise, under the same external force, the peak value of the four-wave mixing spectrum will decrease, and the reduced energy is used for pattern splitting at the resonance (Fig. 7).

Conclusions In this paper, based on the optomechanical systems, a hybrid spinning optomechanical system is proposed. By controlling the rotation speed and direction of the optomechanical cavity, the frequency shift induced by the rotation and the optical bistable behavior can be controlled effectively. The results indicate that the rotating direction and rotation rate of the optomechanical cavity affect the four-wave mixing intensity of the system. The decrease or increase of the four-wave mixing intensity will enhance or suppress the mode splitting phenomenon in the resonance region of the system. The external force will destroy the symmetry of the four-wave mixing spectrum. Moreover, the increase of external force will significantly increase the intensity of the four-wave mixing at a fixed rotation rate. However, under the same external force, the increase of rotation rate will reduce the four-wave mixing intensity of the system. Although the optical bistability and four-wave mixing phenomena have been studied in some optical systems, these two phenomena have not yet been analyzed in spinning optomechanical systems, and the study of nonlinear optical properties of hybrid spinning optomechanical systems will have potential applications in quantum information networks.

Key words nonlinear optics; spinning optomechanical systems; Sagnac effect; optical bistability; four-wave mixing